The FEBS Journal

FEBS PRESS science publishing by scientists

Stress exposure in the *mdx* mouse model of Duchenne muscular dystrophy provokes a widespread metabolic response

Erynn E. Johnson and James M. Ervasti

Department of Biochemistry, Molecular Biology, and Biophysics, University of Minnesota Twin Cities, Minneapolis, MN, USA

Keywords
biological stress; Duchenne muscular dystrophy; metabolism; metabolomics; skeletal muscle

Correspondence
J. M. Ervasti, Paul and Sheila Wellstone Muscular Dystrophy Center, University of Minnesota, 6-155 Jackson Hall, 321 Church St SE, Minneapolis, MN 55455, USA
Tel: 612-626-6517
E-mail: jervasti@umn.edu

(Received 23 July 2024, revised 13 December 2024, accepted 7 February 2025)

doi:10.1111/febs.70029

Duchenne muscular dystrophy is a severe neuromuscular wasting disease that is caused by a primary defect in dystrophin protein and involves organism-wide comorbidities such as cardiomyopathy, metabolic and mitochondrial dysfunction, and nonprogressive cognitive impairments. Physiological stress exposure in the *mdx* mouse model of Duchenne muscular dystrophy results in phenotypic abnormalities that include locomotor inactivity, hypotension, and increased morbidity. Severe and lethal stress susceptibility in *mdx* mice corresponds to metabolic dysfunction in several coordinated metabolic pathways within dystrophin-deficient skeletal muscle, as well as prolonged elevation in *mdx* plasma corticosterone levels that extends beyond the wild-type (WT) stress response. Here, we performed a targeted mass spectrometry-based plasma metabolomics screen focused on biological stress pathways in healthy and dystrophin-deficient *mdx* mice exposed to mild scruff stress. One-third of the stress-relevant metabolites interrogated displayed significant elevation or depletion in *mdx* plasma after scruff stress and were restored to WT levels by skeletal muscle-specific dystrophin expression. The metabolic pathways of *mdx* mice altered by scruff stress are associated with regulation of the hypothalamic–pituitary–adrenal axis, locomotor tone, neurocognitive function, redox metabolism, cellular bioenergetics, and protein catabolism. Our data suggest that a mild stress triggers an exaggerated, multi-system metabolic response in *mdx* mice.

Introduction

Stress pathology in the *mdx* mouse model of Duchenne muscular dystrophy (DMD) was initially published by Sekiguchi *et al.* [1] with the observation of *mdx* scruff restraint-induced freezing behavior. Additional studies have demonstrated that *mdx* stress pathology ranges from sustained tonic immobility and motor inhibition to anxiety-related behaviors and impaired fear memory [2–5]. Our group has reinforced and extended these findings to show that graded *mdx* stress pathology includes inactivity, hypotension,

Abbreviations
2-AG, 2-arachidonoylglycerol; AA, arachidonate; AEA, *N*-arachidonoylethanolamine/anandamide; BCAA, branched-chain amino acid; BCAT, branched-chain amino acid aminotransferase; BCKA, branched-chain α-ketoacid; cAMP, cyclic adenosine monophosphate; CB, cannabinoid; Cort, corticosterone; DCM, differentially circulating metabolite; DMA, dimethylarginine; DMD, Duchenne muscular dystrophy; EC, endocannabinoid; FAAH, fatty acid amide hydrolase; GPx, glutathione peroxidase; GR, glucocorticoid receptor; GSH, reduced glutathione; GSSG, oxidized glutathione; HPA, hypothalamic–pituitary–adrenal; i.c.v., intracerebroventricular; i.p., intraperitoneal; LEA, linoleoyl ethanolamide; MR, mineralocorticoid receptor; mTOR, mammalian target of rapamycin; OEA, oleoyl ethanolamine; OT, *N*-oleoyl taurine; PC, phosphatidylcholine; PCA, principal component analysis; PE, phosphatidylethanolamine; SkM, skeletal muscle; TRP, transient receptor potential; WT, wild-type; XDH/XO, xanthine dehydrogenase/oxidase; ZT, Zeitgeber time.

and lethality that is rescued by restoration of skeletal muscle (SkM)-specific dystrophin expression [6,7]. DMD patients have also been shown to exhibit stress hypersensitivity [8], which may impact disease course given the chronic physical and emotional stress associated with a lethal neurodegenerative disease. Although *mdx* stress response phenomena are reproducible and potential neural and endocrine mechanisms have been discussed [3,6,9,10], the biochemical underpinnings of poor *mdx* stress outcomes are currently unknown. The mild nature of scruff stress and its reproducible effect on *mdx* locomotor activity presents an opportunity to understand the pathomechanism of *mdx* stress behavior without lethal stress perturbation, with potential translation to safe and ethical physiological stress studies conducted in DMD patients [8]. In this study, we sought to identify novel candidate metabolites that may mediate the *mdx* stress response with potential for validation in future work as stress biomarkers and therapeutic targets in both murine and human forms of DMD.

We employed a commercial biological stress-targeted metabolomics panel to quantify stress-relevant metabolites that are uniquely altered in *mdx* circulation upon physiological stress exposure. The selected plasma metabolomics screen included over 100 metabolites chosen based on literature review and collectively linked to seven biological stress pathways: inflammation and immunity, stress signaling, injury and circulation, oxidative stress, metabolism and glycemic stress, protein catabolism and decay, and vitamins. To provide a benchmark for the influence of SkM dystrophin expression upon stress-relevant circulating metabolome alterations and to identify metabolic pathway mediators relevant to *mdx* stress phenotypes, we included the MTBD/*mdx* mouse in our metabolomics panel as a transgenic model that restores dystrophin expression exclusively to the SkM compartment and rescues *mdx* stress pathophysiology. Our investigation demonstrated a unique stress-dependent change in one-third of all analyzed stress metabolites in the *mdx* plasma metabolome. Among the metabolic changes in *mdx* circulation following stress are metabolites that participate in neurological signaling, locomotor tone, hypothalamic–pituitary–adrenal (HPA) axis regulation, glucose metabolism and bioenergetic homeostasis, protein catabolism, and redox metabolism. Our data identified a unique stress-dependent circulating metabolome in *mdx* mice, yielding new leads for metabolic candidates that contribute to *mdx* stress pathology and demonstrating a striking role for SkM in the regulation of central stress metabolic pathways.

Results

Stress-induced shifts in plasma metabolome are dependent on SkM dystrophinopathy

We commissioned a targeted metabolomics panel through Metabolon (Research Triangle Park, Morrisville, NC, USA) with a curated list of metabolites that were selected based on their contributions to biological stress signaling pathways. Our group and others have demonstrated that brief 10–30 s scruff restraint causes prolonged inactivity in *mdx* mice ranging from 3 to 6 months of age, representing a reproducible nonlethal *mdx* stress response is robust to variability due to experimenter and technique [1,2,6,10,11]. Plasma from wild-type (WT), *mdx*, and SkM dystrophin-replete MTBD/*mdx* mice was collected at baseline or 30 min following 30 s scruff exposure (Fig. 1A), a time point at which corticosterone (Cort) has been demonstrated to remain elevated in *mdx* mice compared to WT mice [6]. All samples (n = 6–9/group) were subjected to LC/MS analysis (Fig. 1B; Data S1). A principal component analysis (PCA) plot of the resulting data showed close clustering of WT and MTBD/*mdx* baseline and post-scruff metabolomes, with *mdx* baseline and post-scruff metabolomes clustering apart from WT and MTBD/*mdx* groups and separation between the *mdx* baseline and post-scruff groups (Fig. 1C). Intergroup variability was primarily accounted for by PC1 and PC2, with 29.9% of the variability in the data explained by PC1 and 14.4% of the variability explained by PC2. Heat map visualization demonstrates an overall pronounced pattern of metabolic shifts in the *mdx* post-scruff plasma metabolome compared to all other groups, including a substantial number of elevated metabolites and several depleted metabolites (Fig. 1D). A total of 23 metabolites were identified as significantly elevated or depleted in the *mdx* post-scruff plasma metabolome; these differentially circulating metabolites (DCMs) are bolded in Fig. 1D and listed in Table 1. Variable correlation plot analysis indicates that urate and taurine are influential metabolites driving the separation of baseline and post-scruff *mdx* groups (Fig. 1E).

Volcano plots were generated for two-group DCM comparisons to visualize patterns and magnitudes of stress- and dystrophin-dependent metabolomic changes (Figs 2 and 3). A total of 19 metabolites were elevated, and three metabolites were depleted in *mdx* compared to WT baseline plasma (Fig. 2A). Similarly, 12 metabolites were elevated and one metabolite was depleted in *mdx* compared to MTBD/*mdx* baseline plasma (Fig. 2C). In contrast, few metabolomic alterations

were observed between WT and MTBD/*mdx* plasma, with five elevated and three depleted metabolites in MTBD/*mdx* compared to WT baseline plasma (Fig. 2E). Scruff stress was associated with a greater magnitude of metabolomic changes between *mdx* and WT or MTBD/*mdx* mice. A total of 41 elevated and two depleted metabolites were observed in *mdx* compared to WT post-scruff plasma (Fig. 2B). We observed an elevation in 23 metabolites and depletion in one metabolite in *mdx* compared to MTBD/*mdx* plasma (Fig. 2D). Similar to our observations in baseline groups, WT and MTBD/*mdx* post-scruff plasma metabolomes were closely aligned, with a total of eight depleted metabolites in MTBD/*mdx* compared to WT post-scruff plasma (Fig. 2F).

Interestingly, scruff stress induced only two significant metabolomic alterations in WT and MTBD/*mdx*, with an elevation in isoleucine and depletion in trigonelline (*N*′-methylnicotinamide) observed in both the WT and MTBD/*mdx* post-scruff metabolomes compared to their respective baseline metabolomes (Fig. 3A,B). In stark contrast, there were many metabolomic changes between the baseline and post-scruff *mdx* plasma metabolomes, with 15 elevated metabolites and three depleted metabolites in *mdx* post-scruff plasma (Fig. 3C). Based on statistical analysis between all six groups for each metabolite, there were a total of 20 uniquely elevated metabolites and three uniquely reduced metabolites in *mdx* post-scruff plasma, representing a significant change in 32% of all analyzed metabolites in the *mdx* post-scruff plasma metabolome (Fig. 3D). Meanwhile, another 22% of metabolites were altered in the *mdx* metabolome independent of stress compared to WT or MTBD/*mdx* plasma (Fig. 3D). The remaining 33 metabolites (46%) were unaltered between groups or demonstrated alterations that were not dependent on SkM dystrophinopathy (Fig. 3D). Overall, our analysis suggests a unique metabolomic shift in *mdx* plasma after scruff stress exposure that involves an increase in many circulating stress-related metabolites. Remarkably, transgenic SkM dystrophin expression in MTBD/*mdx* mice rescued scruff-induced *mdx* metabolomic changes and restored a near WT-like plasma metabolome at baseline and after scruff stress.

Corticosterone elevation in *mdx* plasma after scruff recapitulates historical data

Based on the broad number of metabolic changes observed in *mdx* post-scruff circulation, we focused our analyses below on pathways that bridge *mdx* and DMD patient metabolic alterations and are most likely to be clinically relevant indicators and targets for DMD stress pathology. However, additional metabolomic data implicating oxylipin, kynurenine, ketone body, and energy metabolism in the stress response of *mdx* mice are available upon request. Elevated Cort levels in *mdx* plasma and adrenal gland hyperactivation following graded forms of physiological stress exposure correlate with pathological and lethal *mdx* stress susceptibility [6,11]. HPA axis signaling activity is mediated through the production of neuroendocrine hormones terminating in the secretion of Cort, which binds to glucocorticoid receptors (GRs) and mineralocorticoid receptors (MRs) throughout the body to stimulate lipolysis and gluconeogenesis, regulate blood pressure, and suppress inflammation for stress response resolution (Fig. 4A). Consistent with our published work, circulating Cort levels were elevated in *mdx* post-scruff plasma compared to WT and MTBD/*mdx* groups (Fig. 4B). Post-scruff hyperglycemia was also observed in *mdx* mice, but not in WT or MTBD/*mdx* mice, likely as a result of increased Cort signaling (Fig. 4C). These data confirm HPA axis hyperactivity in *mdx* mice following scruff stress that is rescued by SkM dystrophin expression.

Chronic glucocorticoid treatment is a standard of care for many DMD patients and can result in suppressed endogenous cortisol production and epigenetic alterations in metabolic programs [12,13]. We treated *mdx* mice using a weekly glucocorticoid (prednisone) pulsing strategy to mimic glucocorticoid treatment in DMD patients and examine the impact of pharmacological HPA axis regulation on *mdx* scruff pathology (Fig. 4D). Our data showed that 4 weeks of intermittent prednisone treatment (1 $mg \cdot kg^{-1}$, i.p.) did not have an effect on *mdx* scruff-induced inactivity (Fig. 4E). Collectively, these data suggest that HPA axis dysregulation and associated scruff stress pathology in *mdx* mice is ameliorated by transgenic SkM dystrophin expression but not exogenous HPA axis modulation with glucocorticoids.

Glutathione, taurine, and xanthine metabolic shifts in *mdx* post-scruff plasma indicate elevated oxidative stress in the *mdx* stress response

Cysteine serves as a precursor to glutathione (GSH) as well as the taurine and transsulfuration pathways (Fig. 5A), which both exhibit defects in a DMD context [14–16]. We observed significantly elevated cysteine levels in *mdx* plasma independent of scruff exposure (Fig. 5B), as well as significantly elevated oxidized cysteine (cystine) levels in *mdx* plasma at baseline that

were reduced after scruff stress (Fig. 5C). Hypotaurine is an intermediate metabolite in the conversion of cysteine to taurine (Fig. 5A) and was elevated in both *mdx* and MTBD/*mdx* plasma at baseline and post-scruff compared to WT plasma (Fig. 5D). In contrast, taurine levels were elevated in *mdx* plasma, with a dramatic additional increase in *mdx* plasma taurine levels following scruff exposure (Fig. 5E). Post-scruff taurine elevation in *mdx* plasma may serve antioxidant roles, but may also reflect impaired taurine transport into

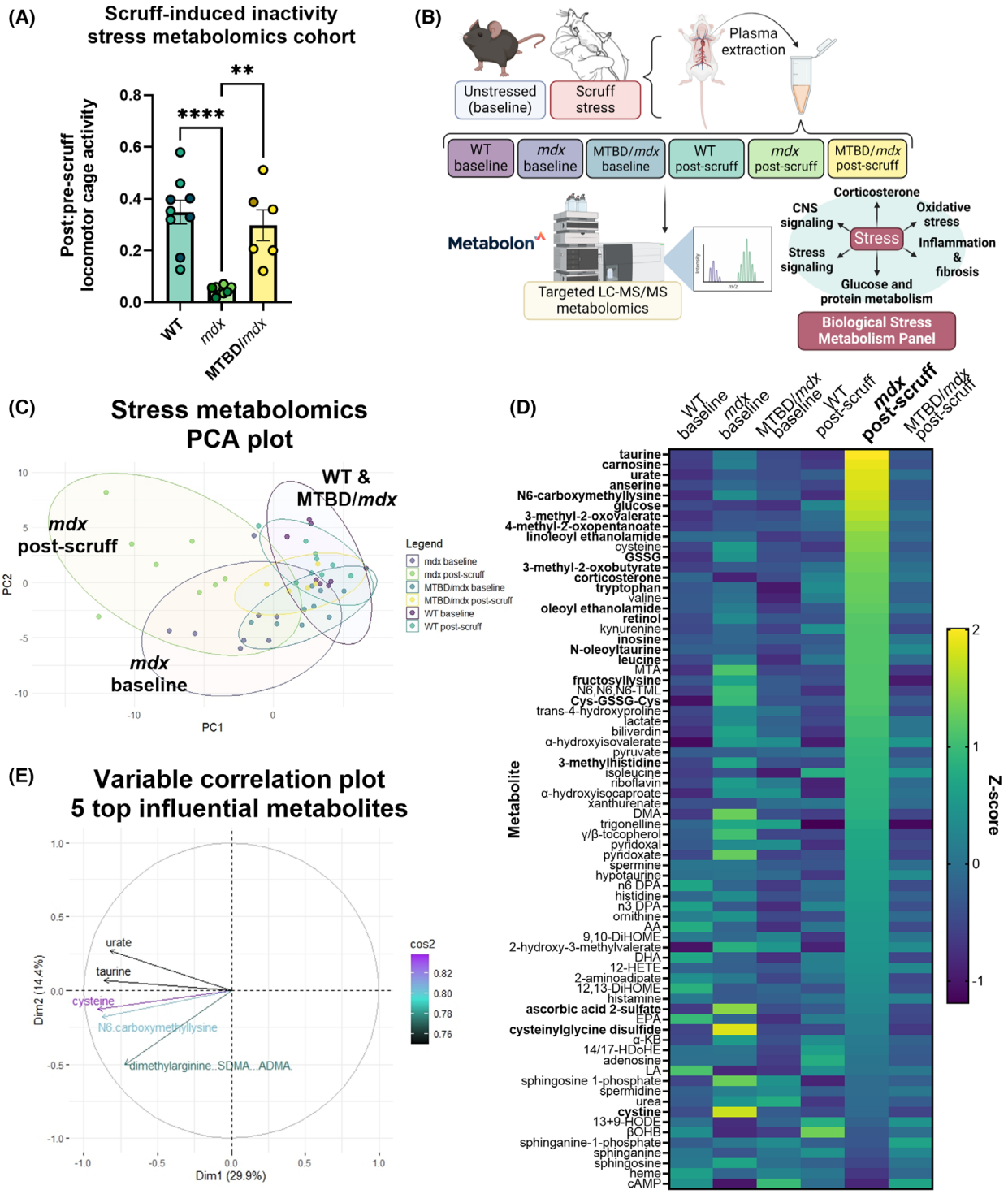

Fig. 1. Plasma metabolomic characterization in healthy and *mdx* mice at baseline and following scruff exposure. (A) Scruff-induced inactivity was measured for wild-type (WT), *mdx*, and MTBD/*mdx* mice as the ratio of total locomotor activity for 30 min before and after 30 s mild scruff restraint. This scruff stress assay has been replicated in *mdx* mice for over a decade and published previously by our laboratory and others [1–6]. Activity measurements were followed by euthanasia and blood collection for biological stress-targeted metabolomics analysis. Comparisons between groups were made using one-way ANOVA with Tukey's multiple comparisons test (**$P < 0.01$; ****$P < 0.0001$). Adjusted *P*-values were determined by Benjamini–Hochberg multiple comparisons hypothesis testing. Bar graph depicts means (±SEM) from $n = 9$ WT mice, $n = 8$ *mdx* mice, and $n = 6$ transgenic MTBD/*mdx* mice. (B) Schematic representation of experimental design and main biological stress pathways analyzed in a biological stress-targeted metabolomics analysis performed in singlicate for WT, *mdx*, and MTBD/*mdx* baseline and post-scruff plasma samples ($n = 8$ baseline WT, $n = 8$ baseline *mdx*, $n = 9$ baseline MTBD/*mdx*, $n = 9$ post-scruff WT, $n = 8$ post-scruff *mdx*, and $n = 6$ post-scruff MTBD/*mdx* mice). (C) Principal component analysis (PCA) plot demonstrates metabolomic similarities and differences between the six experimental groups. (D) Heat map display of group *z*-scores for the 72 biological stress metabolites identified in the metabolomics screen. Heat map *z*-scores were calculated as group z-score averages using the row mean and population standard deviation for each metabolite. Illustrations were made in BioRender. (E) Variable correlation plot depicts the top five metabolites that contribute to variability in the PCA plot. CNS, central nervous system; LC–MS/MS, tandem liquid chromatography-mass spectrometry.

Table 1. Metabolites with significantly altered levels in *mdx* post-scruff plasma. Statistical comparisons were made with two-way ANOVA and Tukey's multiple comparisons *post hoc* test.

Metabolite	Elevated/depleted (main effect or interaction p-value)
Corticosterone	Elevated ($P = 0.004$)
Oxidized glutathione (GSSG)	Elevated ($P = 0.01$)
Taurine	Elevated ($P < 0.0001$)
Carnosine	Elevated ($P < 0.0001$)
Anserine	Elevated ($P < 0.0001$)
Glucose	Elevated ($P = 0.0001$)
N^6-carboxymethyllysine	Elevated ($P < 0.0001$)
Urate	Elevated ($P < 0.0001$)
Trp	Elevated (main effect $P < 0.001$)
α-ketomethylvalerate	Elevated ($P < 0.0001$)
α-ketoisocaproate	Elevated ($P < 0.0001$)
α-ketoisovalerate	Elevated ($P = 0.03$)
3-methylhistidine	Elevated (main effect $P < 0.01$)
Fructosyllysine	Elevated ($P = 0.002$)
Retinol	Elevated (main effect $P < 0.0001$)
Linoleoyl ethanolamide	Elevated ($P < 0.0001$)
Oleoyl ethanolamide	Elevated ($P = 0.0006$)
N-oleoyl taurine	Elevated (main effect $P < 0.01$)
Leucine	Elevated (main effect $P < 0.01$)
Inosine	Elevated ($P = 0.005$)
Cystine	Depleted ($P = 0.0003$)
Cysteinylglycine disulfide	Depleted ($P < 0.0001$)
Ascorbic acid 2-sulfate	Depleted ($P = 0.03$)

dystrophin-deficient SkM to provide cytoprotection against oxidative stress [15,17]. Taurine also possesses vasodilatory signaling functions [18], suggesting that its drastic elevation in *mdx* plasma following scruff may contribute to hypotension.

The recycling of GSH between its reduced and oxidized (GSSG) forms is critical to the cellular antioxidant system (Fig. 5A), and increased oxidative stress leads to an elevated GSSG/GSH ratio in *mdx* mice and DMD patients [14,19,20]. We observed a main effect elevation in *mdx* post-scruff GSSG levels (Fig. 5F). Our data suggest that oxidative stress is elevated in *mdx* mice following stress, with potential increased tissue uptake of cystine for intracellular GSH repletion and increased antioxidant capacity [21]. In addition to cysteine and GSH metabolic intermediates, the biological stress metabolomics panel revealed alterations in purine metabolism (Fig. 5H), a pathway that has previously been implicated in *mdx* SkM and cardiac pathology [22,23]. Adenosine is a precursor of xanthine and was reduced in MTBD/*mdx* plasma overall (Fig. 5G). In addition to its substrate role in xanthine metabolism, adenosine can also signal via adenosine receptors to modulate the production of cyclic adenosine monophosphate (cAMP), which contributes to a multitude of physiological processes including SkM hypertrophy, vasodilation, and cell growth [24,25]. Levels of cAMP were reduced in *mdx* plasma, regardless of scruff exposure (Fig. 5I). Inosine and urate are adenosine catabolites whose levels were uniquely elevated in *mdx* post-scruff plasma (Fig. 5J, L). Xanthine was not detected in our analysis and the abundance of its direct precursor, hypoxanthine, was highly variable and unchanged among groups (Fig. 5K).

Scruff stress modulates circulating endocannabinoid levels in *mdx* mice

Several endogenous cannabinoid, or endocannabinoid (EC), metabolites were identified in the biological stress discovery metabolomics panel. Phospholipid-derived EC biogenic lipids bind cannabinoid (CB) receptors 1 and 2 that are differentially expressed throughout the body, as well as vanilloid/transient receptor potential (TRP) channels receptors and β1-adrenergic receptors (Fig. 6A). EC receptor-mediated

signaling regulates a multitude of cellular and physiological functions including motor activity, afferent neurotransmission, inflammation, and oxidative metabolism [26]. The most extensively studied EC metabolites are *N*-arachidonoylethanolamide (anandamide; AEA) and 2-arachidonoylglycerol (2-AG), which

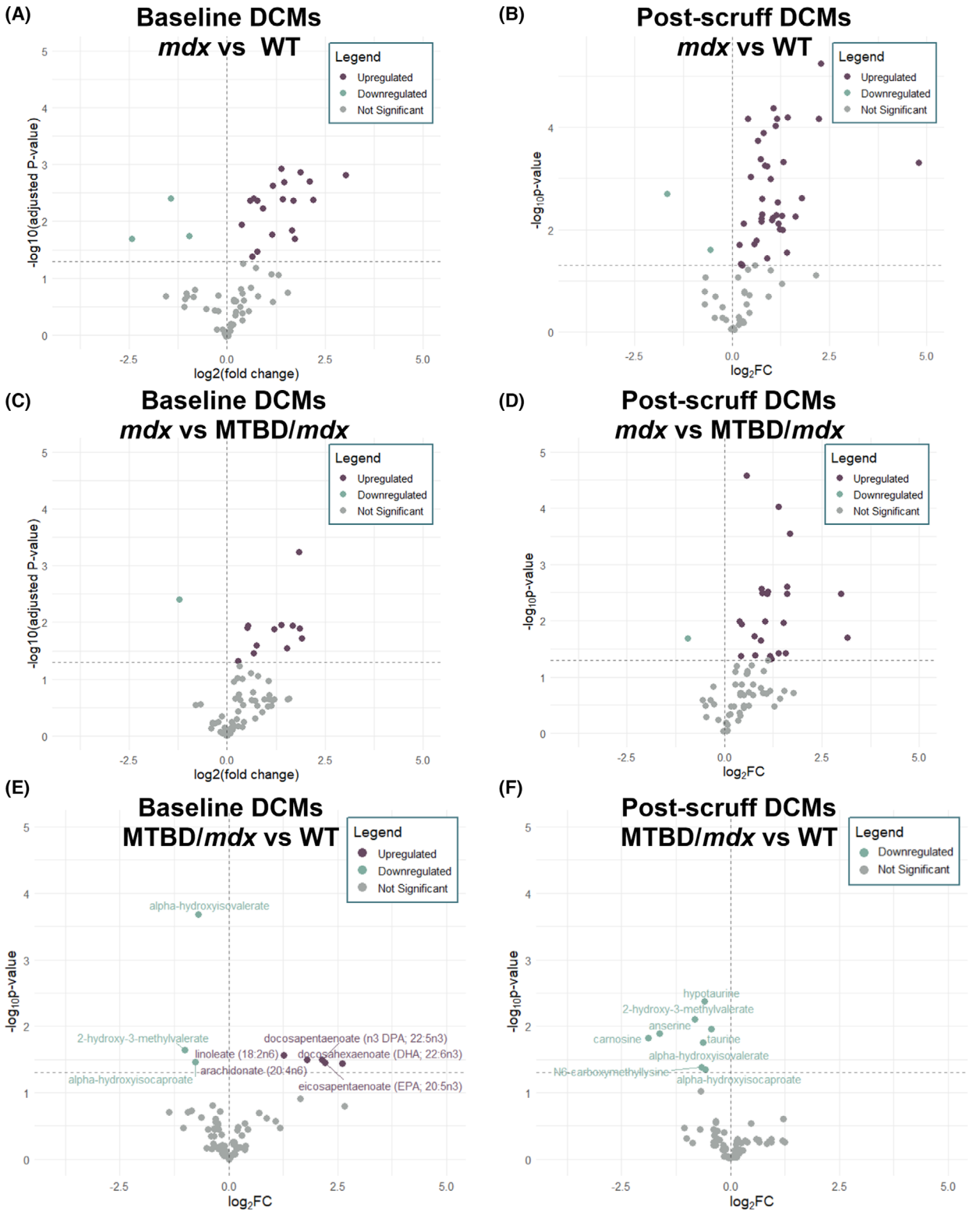

Fig. 2. Volcano plots identify metabolites with significantly different abundance in two-group comparisons between *mdx* and wild-type (WT) or *mdx* and MTBD/*mdx* at baseline and post-scruff. Differentially circulating metabolites (DCMs) were characterized as upregulated or downregulated based on an adjusted *P*-value less than 0.05 for (A) baseline *mdx* vs wild-type (WT) comparisons, (B) post-scruff *mdx* vs WT comparisons, (C) baseline *mdx* vs transgenic MTBD/*mdx* comparisons, (D) post-scruff *mdx* vs MTBD/*mdx* comparisons, (E) baseline MTBD/*mdx* vs WT comparisons, and (F) post-scruff MTBD/*mdx* vs WT comparisons. Adjusted *P*-values were determined by Benjamini–Hochberg multiple comparisons hypothesis testing and volcano plots were plotted as $\log_2$(fold change) vs $-\log_{10}$(adjusted *P*-value). Experimental groups were comprised of $n = 8$ baseline WT, $n = 8$ baseline *mdx*, $n = 9$ baseline MTBD/*mdx*, $n = 9$ post-scruff WT, $n = 8$ post-scruff *mdx*, and $n = 6$ post-scruff MTBD/*mdx* mice.

are derived from phospholipids (Fig. 6A) [26]. However, neither AEA nor 2-AG were identified among our plasma samples. Three alternative ECs were identified in our study and were significantly elevated in *mdx* post-scruff plasma, including taurine-derived *N*-oleoyl taurine (OT), phosphatidylethanolamine (PE)-derived oleoyl ethanolamide (OEA), and phosphatidylcholine (PC)-derived and linoleoyl ethanolamide (LEA) (Fig. 6B–D). As shown in Fig. 4E, taurine was also significantly elevated in *mdx* post-scruff circulation, indicating a potential role for taurine and EC metabolic flux in biosynthetic organs including the liver, which expresses the putative OT synthetic enzyme, *N*-acetyltransferase [27,28]. Amidated lipids OT, OEA, and LEA are degraded by fatty acid amide hydrolase (FAAH) to arachidonate (AA) (Fig. 6A), which demonstrated reduced circulating levels in MTBD/*mdx* mice compared to WT mice, while *mdx* mice displayed intermediate AA levels at baseline and WT-like AA levels after scruff stress (Fig. 6E). This result suggests that EC metabolite elevation in *mdx* post-scruff plasma is not due to inhibition of FAAH activity and points instead to an upregulation of upstream EC metabolic activity in one or more biosynthetic tissues as part of the *mdx* stress response.

Protein catabolism markers are elevated in *mdx* mice and branched-chain amino acid metabolites are elevated post-scruff

Finally, our analysis revealed alterations in metabolites associated with protein catabolism (Fig. 7A) in the *mdx* plasma metabolome. SkM degradation marker 3-methylhistidine was elevated in *mdx* post-scruff plasma (Fig. 7B), while histidine levels were unchanged among groups (Fig. 7C). Carnosine and anserine are dipeptide signaling molecules derived from 3-methylhistidine (Fig. 7A) that were found to be significantly elevated in *mdx* post-scruff plasma (Fig. 7D, E). Meanwhile, histidine-derived histamine was not altered among groups (Fig. 7F). Dimethylarginine (DMA; sum of symmetrical DMA and asymmetrical DMA abundances) is another protein degradation marker and demonstrated scruff-independent elevation in *mdx* plasma (Fig. 7G). Similarly, trans-4-hydroxyproline and N^6,N^6,N^6-trimethyllysine were elevated in *mdx* plasma regardless of scruff exposure (Fig. 7H,I).

Branched-chain amino acids (BCAAs) leucine, isoleucine, and valine regulate SkM mass, protein breakdown, and mammalian/mechanistic target of rapamycin (mTOR)-mediated anabolic processes (Fig. 8A) [29]. Leucine and valine exhibited stress-dependent elevation in *mdx* plasma (Fig. 8B,D), while circulating isoleucine was elevated after scruff in WT, *mdx*, and MTBD/*mdx* plasma (Fig. 8C). BCAAs are metabolized by branched-chain aminotransferases (BCATs) to BCAA α-ketoacids (BCKAs): α-ketoisocaproate, α-keto-β-methylvalerate, and α-ketoisovalerate (Fig. 8A) [29], which were each dramatically elevated uniquely in *mdx* post-scruff plasma (Fig. 8E–G). BCKAs are further metabolized to enter the TCA cycle by the BCKA dehydrogenase complex or are alternatively reduced by hydroxy acid dehydrogenases to form α-hydroxyisocaproate, α-hydroxy-β-methylvalerate, and α-hydroxyisovalerate (Fig. 8A). These reduced BCAA products displayed elevated circulating levels in both *mdx* and MTBD/*mdx* mice, independent of scruff exposure (Fig. 8H–J). These data indicate that protein catabolism is basally elevated in *mdx* mice, and amino acid derivatives carnosine, anserine, and BCKAs demonstrate unique hyperaccumulation in *mdx* plasma following scruff stress.

Discussion

We performed a biological stress metabolomics assay that verified several known stress biomarkers and identified many novel metabolic shifts in *mdx* plasma following a brief scruff stress exposure. Cort elevation in *mdx* post-scruff plasma aligns with our previous data [6] and coincided with post-scruff hyperglycemia in *mdx* plasma, suggesting that stress-perturbed *mdx* mice exhibit HPA axis hyperactivation. Our data show that exogenous glucocorticoid treatment in *mdx* mice to mimic standard DMD corticosteroid therapy [30,31]

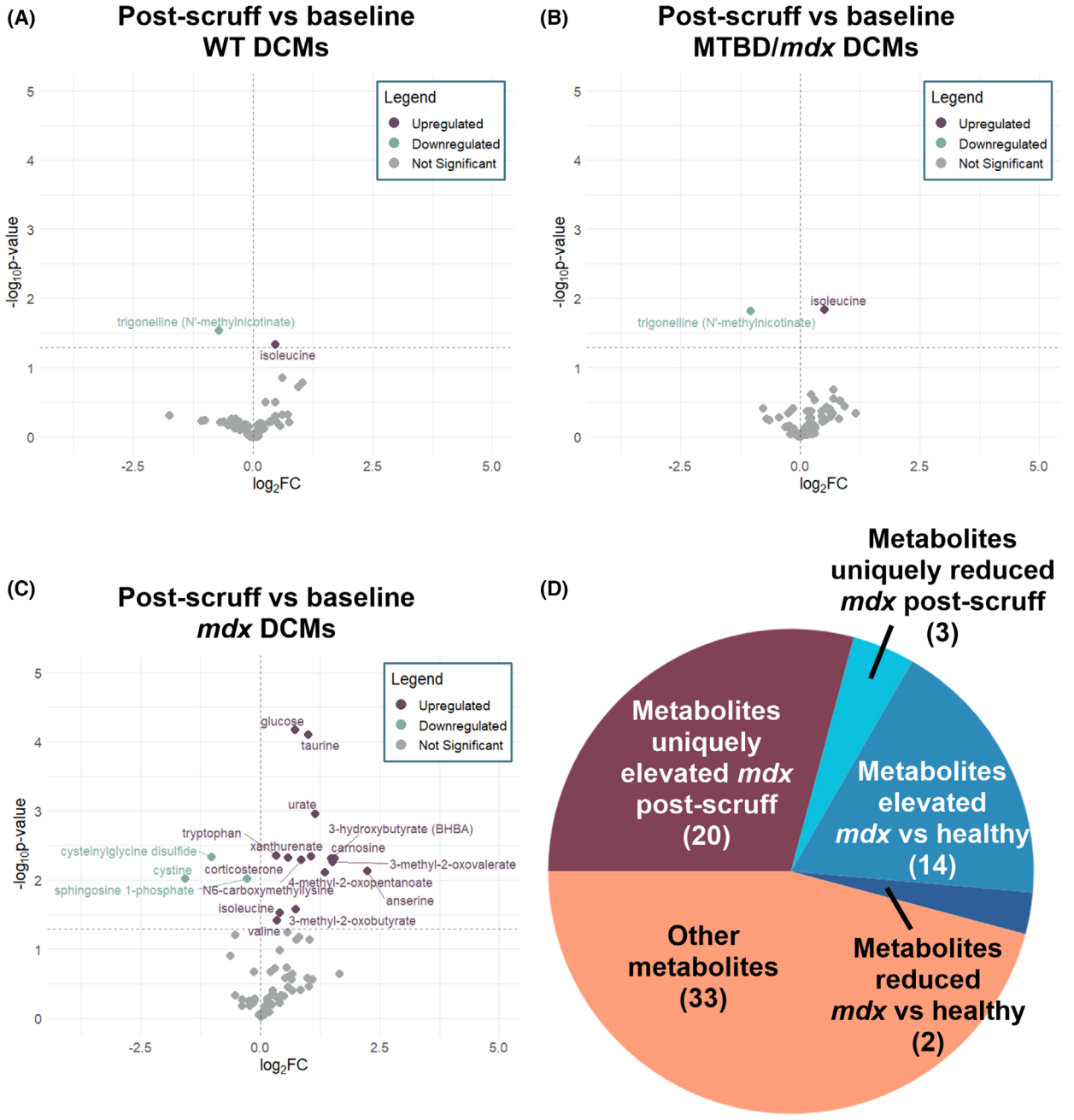

Fig. 3. Volcano plots identify metabolites with significantly different abundance in two-group intra-genotype comparisons between baseline and scruff conditions. Differentially circulating metabolites (DCMs) were characterized as upregulated or downregulated based on an adjusted *P*-value less than 0.05 for (A) baseline vs post-scruff wild-type (WT) comparisons, (B) baseline vs post-scruff transgenic MTBD/*mdx* comparisons, and (C) baseline vs post-scruff *mdx* comparisons. (D) Proportional plasma metabolomic trends in *mdx* mice at baseline and post-scruff are displayed in a pie chart. Adjusted *P*-values were determined by Benjamini–Hochberg multiple comparisons hypothesis testing and volcano plots were plot as $\log_2$(fold change) vs $-\log_{10}$(adjusted *P*-value). Experimental groups were comprised of $n = 8$ baseline WT, $n = 8$ baseline *mdx*, $n = 9$ baseline MTBD/*mdx*, $n = 9$ post-scruff WT, $n = 8$ post-scruff *mdx*, and $n = 6$ post-scruff MTBD/*mdx* mice.

does not impact the severity of scruff-induced inactivity in *mdx* mice. Previous work by our group shows that adrenal suppression in *mdx* mice with pharmacological inhibitors does not prevent *mdx* scruff-induced inactivity [11]. Our previous and current studies suggest that exogenous HPA axis modulation

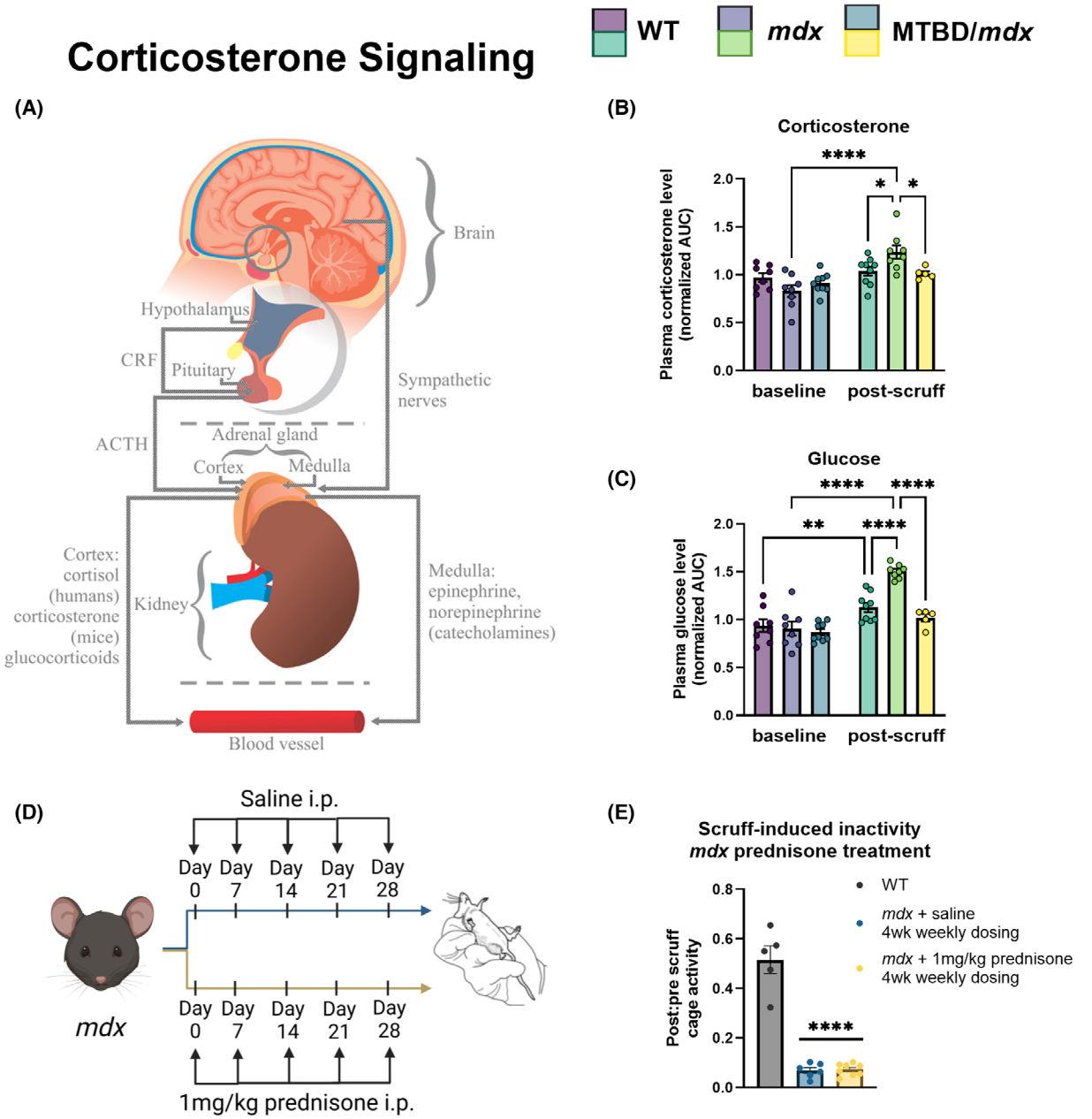

Fig. 4. Endogenous corticosterone is elevated during *mdx* stress response and scruff-induced inactivity is not affected by exogenous glucocorticoid administration. (A) Schematic representation of neuroendocrine hypothalamic–pituitary–adrenal (HPA) and sympatho-adrenal medullary (SAM) axis stress response signaling pathways. ('Response to stress' by Campos-Rodríguez R, Godínez-Victoria M, Abarca-Rojano E, Pacheco-Yépez J, Reyna-Garfias H, Barbosa-Cabrera RE, Drago-Serrano ME is licensed under CC BY 3.0). Corticosterone (Cort) (B) and glucose (C) levels in wild-type (WT), *mdx*, and transgenic MTBD/*mdx* plasma at baseline and following scruff stress exposure were determined by liquid chromatography-mass spectrometry (LC–MS) targeted metabolomics analysis. Bar graphs depict means (±SEM) from $n = 8$ baseline WT, $n = 8$ baseline *mdx*, $n = 9$ baseline MTBD/*mdx*, $n = 9$ post-scruff WT, $n = 8$ post-scruff *mdx*, and $n = 6$ post-scruff MTBD/*mdx* mice. (D) Schematic representation of intermittent glucocorticoid treatment and scruff stress paradigm in *mdx* mice. Mice were treated once per week for 4 weeks with saline or prednisone (1 mg·kg^{-1} i.p.) and subsequently subjected to 30 s scruff stress with pre- and post-scruff activity monitoring. (E) Scruff-induced inactivity was measured as the ratio of total locomotor activity for 30 min before and after a 30 s mild scruff restraint for *mdx* mice treated with saline ($n = 6$) or prednisone ($n = 8$). Untreated WT mice ($n = 5$) were included in scruff stress analysis as a healthy control group. Bar graph depicts mean values (±SEM). Comparisons between groups were made using one- or two-way ANOVA with Tukey's multiple comparisons test (*$P < 0.05$; **$P < 0.01$; ****$P < 0.0001$). ACTH, adrenocorticotropic hormone; CRF, corticotropin releasing factor.

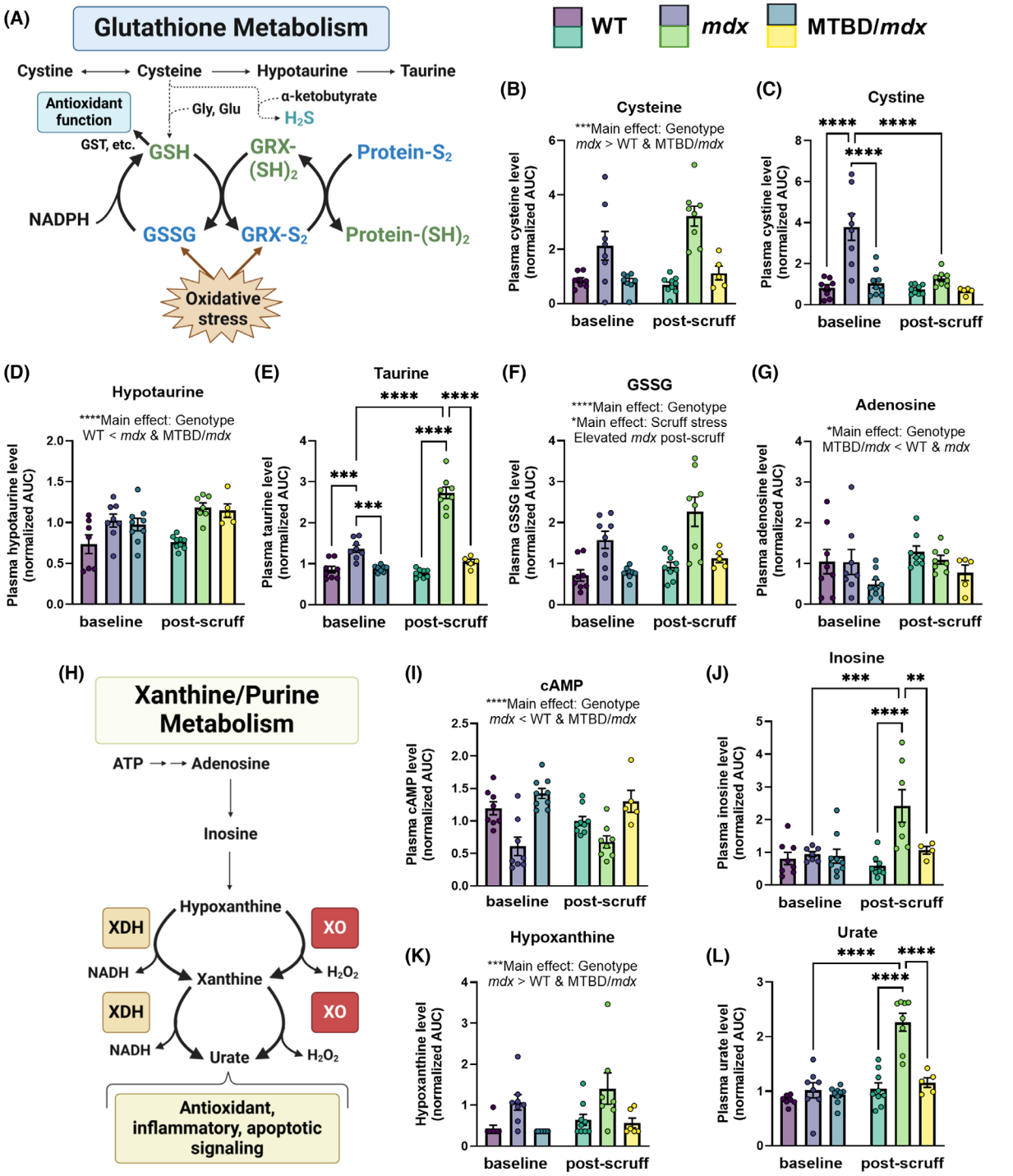

Fig. 5. Circulating glutathione and xanthine metabolic pathway alterations were associated with stress and skeletal muscle dystrophinopathy. (A, H) Schematic representations of (A) glutathione (GSH) and (H) xanthine metabolism. (B) Cysteine, (C) cystine, (D) hypotaurine, (E) taurine, (F) oxidized GSH (GSSG), (G) adenosine, (I) cyclic adenosine monophosphate (cAMP), (J) inosine, (K) hypoxanthine, and (L) urate levels in wild-type (WT), *mdx*, and transgenic MTBD/*mdx* plasma at baseline and following scruff stress exposure were determined by liquid chromatography-mass spectrometry (LC–MS) targeted metabolomics analysis. Bar graphs depict mean values (±SEM) from $n = 8$ baseline WT, $n = 8$ baseline *mdx*, $n = 9$ baseline MTBD/*mdx*, $n = 9$ post-scruff WT, $n = 8$ post-scruff *mdx*, and $n = 6$ post-scruff MTBD/*mdx* mice. Comparisons between groups were made using two-way ANOVA with Tukey's multiple comparisons test (*$P < 0.05$; **$P < 0.01$; ***$P < 0.001$; ****$P < 0.0001$). Illustrations made with BioRender.

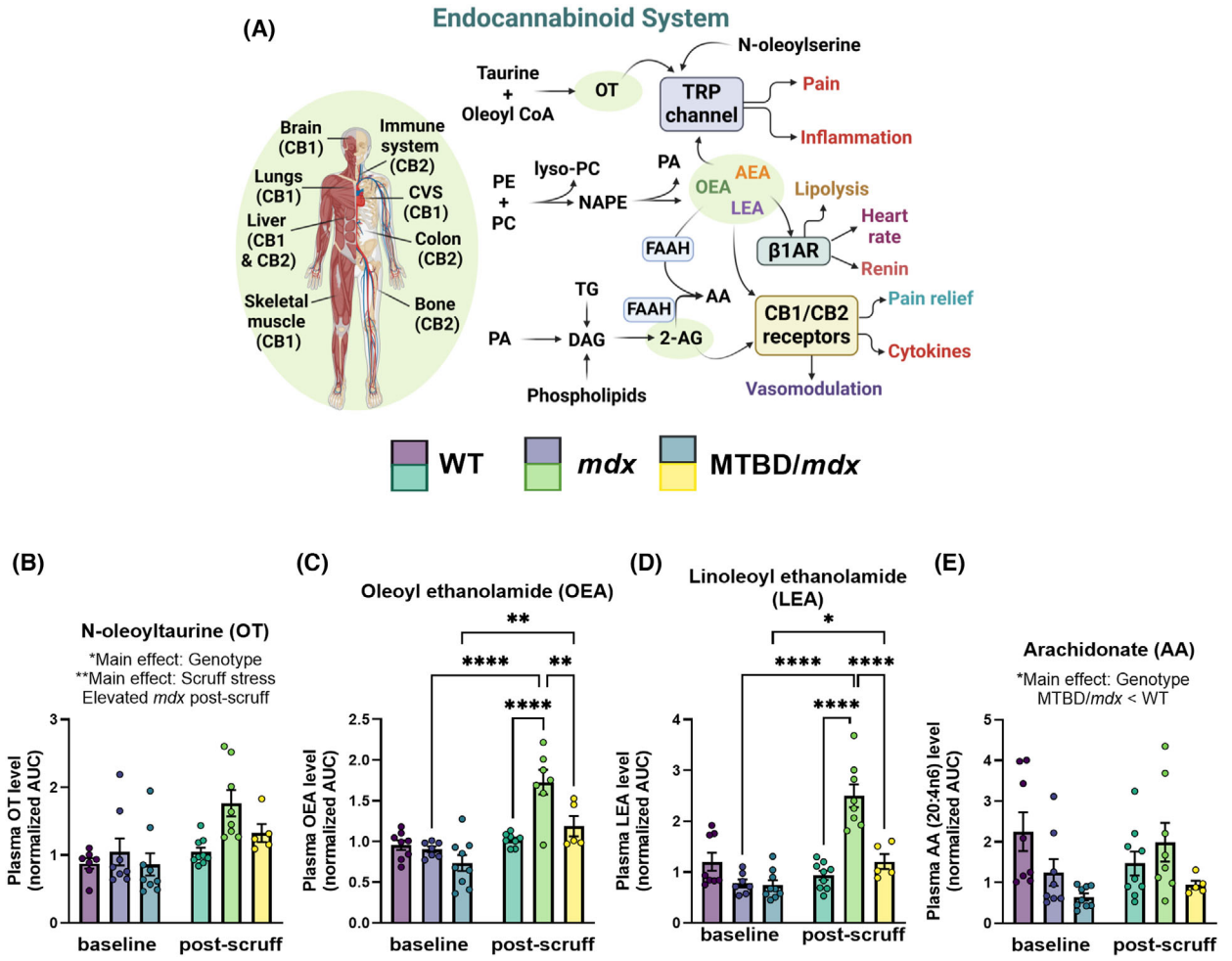

Fig. 6. Circulating endocannabinoid metabolite levels correspond to *mdx* scruff exposure. (A) Schematic representation of endocannabinoid (EC) metabolism. (B) *N*-oleoyl taurine (OT), (C) oleoyl ethanolamide (OEA), (D) linoleoyl ethanolamide (LEA), and (E) arachidonate (AA) metabolites in wild-type (WT), *mdx*, and transgenic MTBD/*mdx* plasma at baseline and following scruff stress exposure were determined by liquid chromatography-mass spectrometry (LC–MS) targeted metabolomics analysis. Bar graphs depict mean values (±SEM) from $n = 8$ baseline WT, $n = 8$ baseline *mdx*, $n = 9$ baseline MTBD/*mdx*, $n = 9$ post-scruff WT, $n = 8$ post-scruff *mdx*, and $n = 6$ post-scruff MTBD/*mdx* mice. Comparisons between groups were made using two-way ANOVA with Tukey's multiple comparisons test (*$P < 0.05$; **$P < 0.01$; ****$P < 0.0001$). Illustrations made with BioRender.

does not target the aberrant regulation of the *mdx* stress response, although the possible roles for Cort as a driver or direct consequence of other observed post-scruff *mdx* plasma metabolomic alterations remain to be distinguished.

Our dataset revealed elevated metabolic markers of oxidative stress in *mdx* mice following scruff stress. Taurine metabolic flux was increased in *mdx* post-scruff circulation, coinciding with elevated cysteine and GSSG levels. Taurine is an antioxidant and is also associated with a range of biological functions, including neuroprotection, immunomodulation, Ca^{2+} homeostasis, energy metabolism, and thermoregulation [21]. Elevated taurine levels in *mdx* plasma could be explained by impaired taurine transport in *mdx* SkM [15,32], resulting in reduced antioxidant defense capacity and elevated *mdx* circulating taurine levels that may cause hypotension through vasodilatory signaling [18]. Increased circulating taurine may also represent increased substrate availability for the EC pathway, as taurine combines with oleoyl CoA to form OT, which was elevated in *mdx* plasma following scruff exposure. Notably, taurine was among the top metabolites in our dataset that discriminated *mdx* post-scruff plasma samples from other groups, emphasizing the magnitude of post-scruff taurine elevation and suggesting

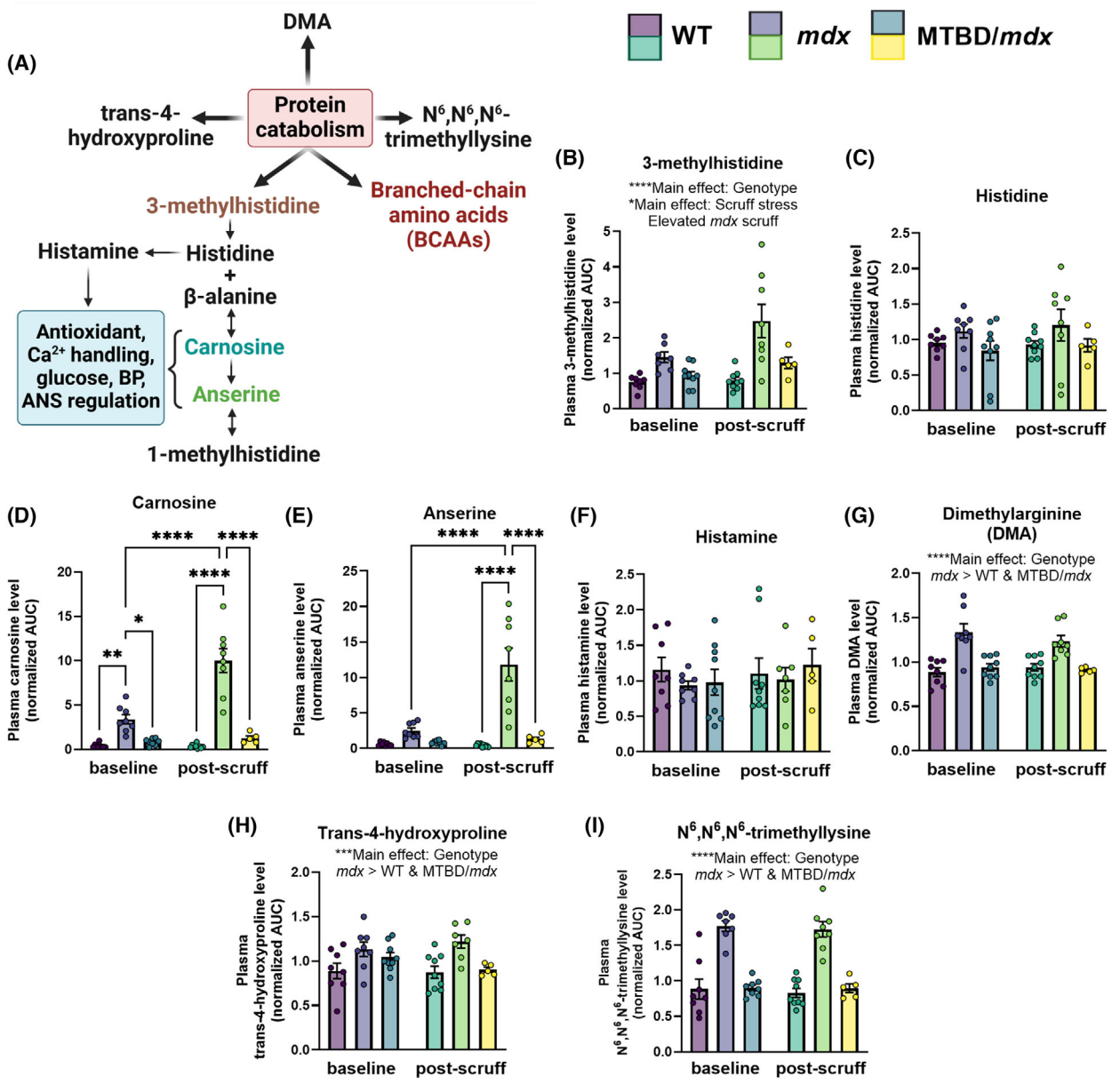

Fig. 7. Circulating metabolic markers of protein catabolism are altered by skeletal muscle dystrophinopathy and scruff exposure. (A) Schematic representation of protein catabolism biomarkers. (B) 3-methylhistidine, (C) histidine, (D) carnosine, (E) anserine, (F) histamine, (G) dimethylarginine (DMA), (H) trans-4-hydroxyproline, and (I) N^6,N^6,N^6-trimethyllysine levels in wild-type (WT), *mdx*, and transgenic MTBD/*mdx* plasma at baseline and following scruff stress exposure were determined by liquid chromatography-mass spectrometry (LC–MS) targeted metabolomics analysis. Bar graphs depict mean values (±SEM) from $n = 8$ baseline WT, $n = 8$ baseline *mdx*, $n = 9$ baseline MTBD/*mdx*, $n = 9$ post-scruff WT, $n = 8$ post-scruff *mdx*, and $n = 6$ post-scruff MTBD/*mdx* mice. Comparisons between groups were made using two-way ANOVA with Tukey's multiple comparisons test (*$P < 0.05$; **$P < 0.01$; ***$P < 0.001$; ****$P < 0.0001$). Illustrations made with BioRender.

that high priority should be given to the further development of this metabolite candidate as an *mdx* biomarker and stress mediator.

We observed elevated purine metabolism and accumulation of purine catabolites inosine and urate in *mdx* post-scruff plasma. Purine metabolism regulates cellular redox status as well as the availability of purine nucleotides necessary for cellular signaling and energy production [33]. Adenosine triphosphate (ATP) is catabolized to adenosine, which is in turn

enzymatically converted to inosine by adenosine deaminase and eliminated in the urine as urate via xanthine metabolism [34]. Urate excretion is elevated in DMD patients, which may be due to increased ATP leakage from damaged dystrophin-deficient SkM and increased purine degradation [35,36]. Elevated circulating CD8/CD26 T cells in DMD patients increase adenosine deaminase binding capacity and enhance adenosine conversion to inosine [37]. Thus, elevated circulating inosine and urate levels in *mdx* mice following scruff exposure may implicate increased sarcolemmal leakiness and immune activation in the *mdx* stress response. Alternatively, specific elevation in xanthine precursor and product metabolites may result from heightened xanthine dehydrogenase/xanthine oxidase (XDH/XO) enzymatic activity in *mdx* SkM that leads to elevated release of the end product, urate, into the circulation. Our laboratory previously demonstrated that XO activity is elevated in *mdx* SkM and is normalized to WT activity levels in MTBD/*mdx* mice [23], supporting a possible function for XO hyperactivity and elevated urate production in *mdx* SkM. Collectively, our results align with previous data that indicates elevated oxidative stress in a dystrophin-deficient state and provide a novel link between stress pathology and established purine metabolic defects in the DMD population.

Our data revealed metabolic alterations indicative of EC system dysfunction in *mdx* mice following scruff stress. EC signaling activity via vanilloid (TRP channel), β1-adrenergic receptors, and CB1/2 receptors influences diverse physiological functions including motor coordination, blood pressure, heart rate, lipolysis, renin and insulin secretion, and inflammation [26–28,38,39]. ECs also perform retrograde signaling in the central and peripheral nervous system via CB1 receptors to modulate nociception, motor tone, memory formation, fear and anxiety-related behaviors, appetite, and energy balance [40]. Elevated SkM CB1 receptor expression has been demonstrated in *mdx* mice and DMD patients [39,41]. Gut dysbiosis in *mdx* mice pathologically elevates EC synthesis and CB1 receptor expression in dystrophin-deficient SkM, which promotes inflammation and impaired autophagy. Gut dysbiosis and EC system dysfunction are counteracted by sodium butyrate treatment that suppresses CB1 and EC synthetic enzyme expression in *mdx* SkM [39].

Relevant to *mdx* stress phenomena, CB2 receptor agonism in rats exposed to a forced swim test was previously shown to reduce immobility time [42]. Microglial CB1 receptor expression is altered by a chronic social defeat stress protocol that we have previously employed to provoke *mdx* lethality [6,43]. Additionally, recent data showed that pharmacological CB2 receptor agonism shifts DMD macrophages toward an anti-inflammatory profile and reduces pro-inflammatory cytokine release [28], suggesting that imbalanced CB1 hyperactivity and CB2 hypoactivity in dystrophin-deficient SkM is deleterious to global physiological function. Altogether, our data suggest that SkM dystrophinopathy influences the circulating levels of ECs during a stress response, which is supported by the observation that MTBD/*mdx* mice restore circulating post-scruff EC abundance to WT levels while concurrently rescuing post-scruff inactivity and hypotension [6].

Elevated protein catabolism is a hallmark of DMD pathological progression and many standard DMD biomarkers are markers of SkM protein degradation [44]. Histidine derivative 3-methylhistidine is a commonly used DMD biomarker that is principally found in SkM actin and myosin proteins and is excreted rather than recycled during muscle catabolism [16]. A recent study identified elevated 3-methylhistidine levels in SkM from stress-susceptible *mdx* mice compared to stress-resilient *mdx* mice [45], corroborating our current data that demonstrate a scruff-dependent elevation in *mdx* circulating 3-methylhistidine levels.

Our BCAA data are in good agreement with previous reports from our laboratory and others that demonstrate elevated urinary or circulating BCAA metabolites in *mdx* mice and DMD patients [46,47]. Valine is elevated in DMD plasma [48], and we observed elevated valine in *mdx* plasma following scruff. According to our data, BCKAs exhibited a specific post-scruff elevation in *mdx* plasma, suggesting a role for these BCAA derivatives in the *mdx* stress signaling axis. Although limited literature exists for the signaling functions of BCKAs, these BCAA derivatives have been linked to elevated oxidative stress, downregulated antioxidant capacity, and impaired cognitive function [49,50]. Of recent interest, cardiac BCKA oxidation via the BCKA dehydrogenase complex was shown to protect against heart failure by adaptive blood pressure reduction [51]. The vasodilatory effects of BCKA oxidized metabolites may serve a pathological role in the hypotensive *mdx* stress response. In combination with stress-dependent alterations in *mdx* purine metabolism, our results point to an elevation in SkM degradation following scruff exposure, which is a surprising result given the mild nature of scruff restraint and subsequent *mdx* hypoactivity that should limit hindlimb SkM damaging contractions. Protein catabolism pathways should be further explored as potential mediators of *mdx* stress pathology.

Regarding the limitations of our study, the metabolite inclusion list was constrained to a subset of

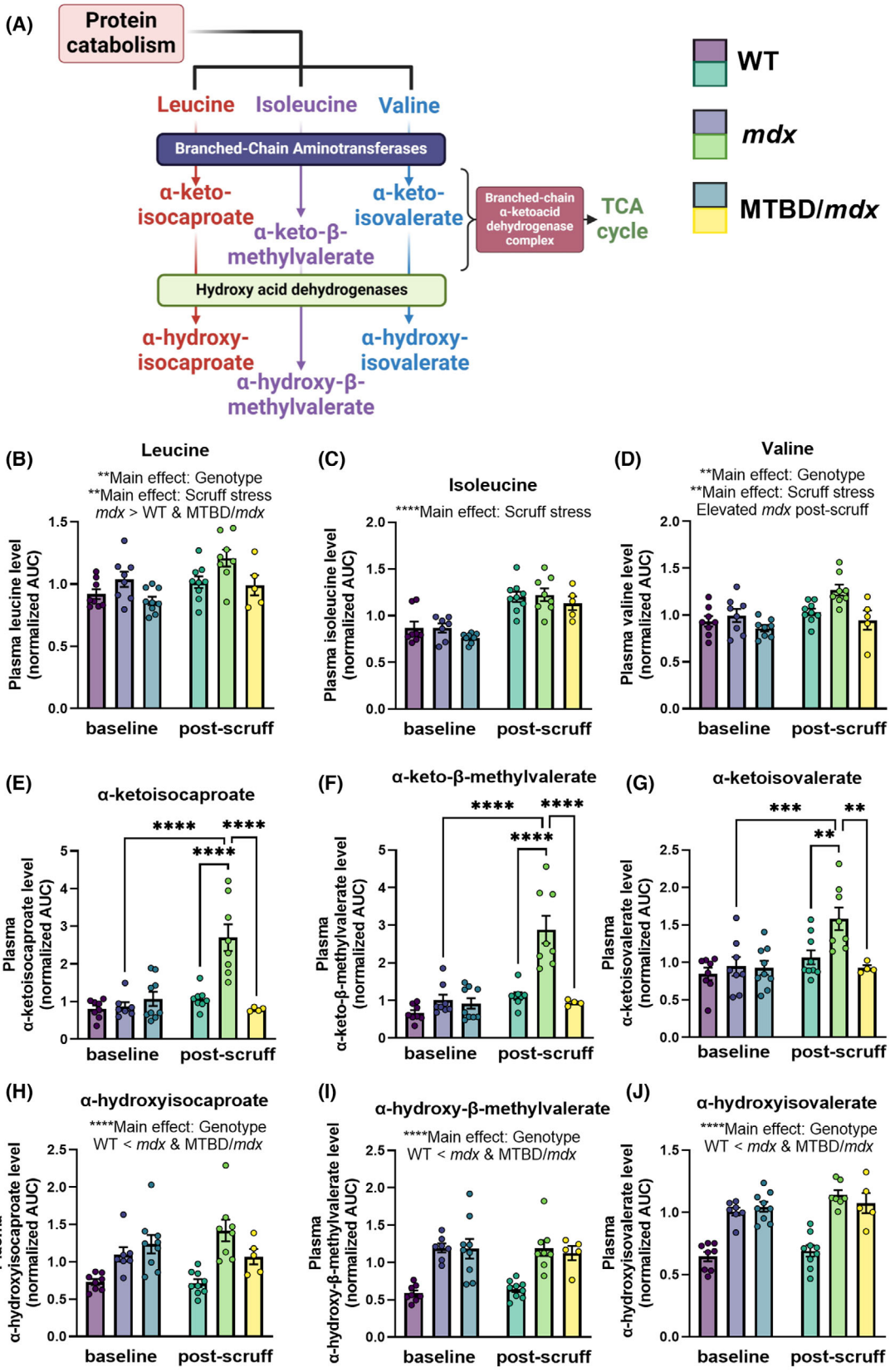
(A)
Protein catabolism
Leucine
Isoleucine
Valine
Branched-Chain Aminotransferases
α-keto-isocaproate
α-keto-β-methylvalerate
α-keto-isovalerate
Branched-chain α-ketoacid dehydrogenase complex
TCA cycle
Hydroxy acid dehydrogenases
α-hydroxy-isocaproate
α-hydroxy-β-methylvalerate
α-hydroxy-isovalerate
WT
mdx
MTBD/mdx
(B)
Leucine
**Main effect: Genotype
**Main effect: Scruff stress
mdx > WT & MTBD/mdx
Plasma leucine level (normalized AUC)
(C)
Isoleucine
****Main effect: Scruff stress
Plasma isoleucine level (normalized AUC)
(D)
Valine
**Main effect: Genotype
**Main effect: Scruff stress
Elevated mdx post-scruff
Plasma valine level (normalized AUC)
(E)
α-ketoisocaproate
Plasma α-ketoisocaproate level (normalized AUC)
(F)
α-keto-β-methylvalerate
Plasma α-keto-β-methylvalerate level (normalized AUC)
(G)
α-ketoisovalerate
Plasma α-ketoisovalerate level (normalized AUC)
(H)
α-hydroxyisocaproate
****Main effect: Genotype
WT < mdx & MTBD/mdx
Plasma α-hydroxyisocaproate level (normalized AUC)
(I)
α-hydroxy-β-methylvalerate
****Main effect: Genotype
WT < mdx & MTBD/mdx
Plasma α-hydroxy-β-methylvalerate level (normalized AUC)
(J)
α-hydroxyisovalerate
****Main effect: Genotype
WT < mdx & MTBD/mdx
Plasma α-hydroxyisovalerate level (normalized AUC)
baseline
post-scruff

Fig. 8. Plasma branched-chain amino acid metabolite levels are regulated by skeletal muscle dystrophinopathy and stress. (A) Schematic representation of branched-chain amino acid (BCAA) metabolism. (B) Leucine, (C) isoleucine, (D) valine, (E) α-ketoisocaproate, (F) α-keto-β-methylvalerate, (G) α-ketovalerate, (H) α-hydroxyisocaproate, (I) α-hydroxy-β-methylvalerate, and (J) α-hydroxyisovalerate levels in wild-type (WT), *mdx*, and transgenic MTBD/*mdx* plasma at baseline and following scruff stress exposure were determined by liquid chromatography-mass spectrometry (LC–MS) targeted metabolomics analysis. Bar graphs depict mean values (±SEM) from $n = 8$ baseline WT, $n = 8$ baseline *mdx*, $n = 9$ baseline MTBD/*mdx*, $n = 9$ post-scruff WT, $n = 8$ post-scruff *mdx*, and $n = 6$ post-scruff MTBD/*mdx* mice. Comparisons between groups were made using two-way ANOVA with Tukey's multiple comparisons test (**$P < 0.01$; ***$P < 0.001$; ****$P < 0.0001$). Illustrations made with BioRender.

potentially stress-relevant metabolites that may be involved in *mdx* stress pathology. For example, the future inclusion of catecholamines that govern sympathetic nervous system stress regulation should be considered to determine the relative impairments in Cort and catecholamine signaling that lead to downstream *mdx* stress susceptibility. Additionally, while the vast majority of metabolite changes in *mdx* mice at baseline and after scruff stress reported here were rescued by muscle-specific transgenic dystrophin expression, we nonetheless identified a small number of metabolites that were not rescued, which suggests a contribution from nonmuscle tissue. We also recently reported evidence suggesting a role for the kynurenine and nicotinamide adenine dinucleotide (NAD^+) pathways in mediating the exaggerated stress response of *mdx* mice [7]. While genetic perturbations corrected kynurenine and NAD^+ metabolic defects in *mdx* mice, they did not rescue the stress phenotypes [7]. Therefore, the metabolic pathways implicated in the current study similarly require validation in engineered mouse models and orthogonal biochemical approaches.

Finally, translational studies are needed to confirm the relevance of *mdx* mild stress biomarkers to the human DMD population. Effective and ethical mild stress exposure has already been demonstrated in DMD patients, and a similar paradigm could be used to collect biofluids from DMD participants before and following a moderate psychosocial stressor to monitor changes in metabolic pathways including EC, oxidative stress, purine, and protein catabolism. Expansion of a DMD stress study to include an untargeted metabolomics screen or a stable isotope labeling approach to investigate metabolic flux would provide further insight into global and tissue-specific metabolic regulation during stress. Particular emphasis should be placed on combining insights from metabolomics data with patient clinical data to identify the correlation between stress exposure, circulating metabolite levels, and key indices of DMD disease progression. In the meantime, our data demonstrate that even a mild stress triggers an exaggerated and widespread metabolic response in *mdx* mice.

Materials and methods

Mice

We used adult male mice in our study between 3 and 4 months of age. Animal care and experimental procedures were approved by the Institutional Animal Care and Use Committee (IACUC) of the University of Minnesota under IACUC protocol #2106-39169A. C57BL6/J and C57BL10/J mice were bred in-house and used as wild-type controls, while C57BL/10ScSn-*Dmd*^{mdx}/J (*mdx*) mice were bred in-house or purchased from The Jackson Laboratory. The MTBD/*mdx* transgenic mouse line [52] expressing a human skeletal actin promotor-driven full-length dystrophin/utrophin chimera with microtubule-binding spectrin repeats 20–24 of dystrophin replaced by nonbinding repeats 18–22 of utrophin was generated in our lab and bred in-house. Mice were group housed following standard specific pathogen free (SPF) procedures with *ad libitum* access to food and water on a 12-h light/dark cycle.

Scruff-induced inactivity

The scruff stress assay was implemented following an established protocol [6,7] in which mice are grasped by the nape of the neck and held horizontally with the tail placed between the palm of the hand and the 5th digit for 30 s. Mice were scruffed at the same time in the morning (ZT1-ZT3) each experimental day to mitigate the confounding influence of circadian fluctuations in endogenous glucocorticoid levels. Following scruff stress and 30-min post-scruff activity monitoring, mice were anesthetized with tribromoethanol (Avertin) and euthanized via cervical dislocation for plasma harvest.

Chronic intermittent glucocorticoid administration

Male *mdx* mice ($n = 8$) were treated once per week for 28 days with prednisone (1 mg·kg^{-1}, i.p.; Millipore Sigma, Burlington, MA, USA) before performing scruff stress and activity monitoring 1 day after the final dose was administered. A control group of *mdx* mice ($n = 6$) was treated in parallel with intraperitoneal saline injections. Mice were treated at 9 am (ZT1) for each dose administered.

Following the final treatment time point, *mdx* mice along with untreated age-matched WT mice were subjected to 30s scruff exposure with 30-min pre- and post-scruff activity monitoring.

Plasma collection

Unhandled and scruff-handled mice were anesthetized with Avertin and cervically dislocated prior to dissection. Blood was collected via cardiac puncture and placed in EDTA-coated anticoagulant tubes. Samples were incubated with end-over-end rotation at room temperature for 15 min, followed by centrifugation for 10 min at 2000 ***g***, 4 °C. Plasma was collected as the supernatant and stored at −80 °C, then underwent one freeze–thaw cycle to aliquot samples for metabolomics analysis.

Metabolomics data acquisition and raw spectral processing

Plasma samples were shipped to Metabolon (Research Triangle Park) for analysis with the custom-built Biological Stress Discovery Panel. The samples were prepared using automated liquid handling equipment to spike plasma with QC recovery standards and to extract metabolites with methanol. The extracted plasma samples were then divided into four fractions for analysis of metabolites with diverse chemical properties using two different reverse-phase (RP)/ultra-high-performance LC (UPLC)-MS/MS-positive mode electrospray ionization (ESI) methods, one RP/UPLC-MS/MS method, and one hydrophilic interaction LC (HILIC)/UPLC-MS/MS method. Samples were dried under vacuum and stored overnight under nitrogen, then reconstituted in compatible solvents for each of the four methods, each containing a series of internal standards at fixed concentrations. All data acquisition was performed utilizing a Waters ACQUITY UPLC (Waters Corp, Milford, MA, USA) and Thermo Scientific Q-Exactive high-resolution/-high-accuracy MS with heated ESI (HESI-II) source and Orbitrap mass analyzer (Thermo Scientific, Waltham, MA, USA) operated at 35000 mass resolution [53].

The first method targeted hydrophilic compounds (PosEarly) using positive ion conditions, a C18 column (Waters UPLC BEH C18-2.1×100 mm, 1.7 μm), and a mobile phase consisting of water, methanol, 0.05% (v/v) perfluoropentanoic acid (PFPA), and 0.1% FA. The second method targeted hydrophobic compounds (PosLate) using positive ion conditions, the same C18 column as employed for the PosEarly method, and a mobile phase consisting of ACN, water, 0.05% PFPA, and 0.01% FA. The third method targeted basic metabolites (Neg) using negative ion mode, a C18 column, and a mobile composed of methanol, water, and 6.5 mM ammonium bicarbonate, pH 8. The fourth method targeted polar metabolites (Polar) using negative ion mode, a HILIC column (Waters UPLC BEH Amide 2.1×150 mm, 1.7 μm), and a mobile composed of water, ACN, and 10 mM ammonium formate, pH 10.8. MS analysis mode altered between MS and data-dependent MS^n scans using dynamic exclusion. The scan range was method-dependent but covered masses between 70 and 1000 m/z. Samples were randomized and balanced for analysis along with extracted water blanks and pooled matrix samples serving as technical replicates.

MS bioinformatics analysis

Raw data files were extracted, peaks were identified, and QC was performed utilizing the Metabolon informatics system that includes a laboratory information management system, data extraction and peak-identification software, data processing tools for QC and analyte identification, and information interpretation and visualization tools for downstream analysis. Compounds were identified by comparison to purified standards or recurrent unknown analytes using a Metabolon-curated library. All identifications required matching based on three criteria for robust and high-accuracy metabolite assignments: retention index within a narrow window, accurate mass match to the library (± 10 ppm), and MS/MS forward and reverse scores between experimental data and authentic standards. The MS/MS scores are based on ion comparison between experimental and library spectra. Peaks were quantified using AUC. Normalization was performed to correct for batch effects during multiple-day instrumental runs. Normalization was performed by median block correction in run-day blocks. Imputation was performed for missing values using the minimum value across all batches in the median-scaled batch-normalized data. Line data are provided as a supplemental data file (Data S1).

Data were presented in an interactive visualization format within the client portal for exploratory data analysis along with spreadsheets containing sample metadata and analyte abundances for client bioinformatics analysis. Batch-normalized and imputed metabolite abundances were used to calculate pairwise fold changes based on the geometric means of all biological replicates from each sample group. Fold changes were calculated for pairwise comparisons between the following groups: *mdx* baseline/WT baseline, *mdx* baseline/MTBD-*mdx* baseline, MTBD-*mdx* baseline/WT baseline, *mdx* post-scruff/WT post-scruff, *mdx* post-scruff/MTBD-*mdx* post-scruff, MTBD-*mdx* post-scruff/WT post-scruff, WT post-scruff/WT baseline, *mdx* post-scruff/*mdx* baseline, and MTBD-*mdx* post-scruff/MTBD-*mdx* baseline. A two-way unpaired Student's *t*-test was used to calculate *P*-values for pairwise fold changes, and the Benjamini–Hochberg method was used to control the false discovery rate (FDR). Corrected *P*-values were log-transformed and plotted against log-transformed fold change values to obtain volcano plots generated in R using the TIDYVERSE package, and a minimum corrected *P*-value

cutoff of 0.05 was applied to identify differentially circulating metabolites (DCMs) in pairwise comparisons. Comparisons between all experimental groups was performed using two-way ANOVA statistical analysis with Tukey's multiple comparisons correction. Full metabolite quantification datasets and lists of DCMs were imported to R for data filtering and visualization using the GPLOTS, VENNDIAGRAM, DPLYR, GGCORRPLOT, FACTOMINER, GGFORTIFY, and GGBIPLOT packages. PCA plots and variable correlation plots were generated to visualize data grouping trends and to identify the most influential metabolites contributing to intergroup variability. Venn diagrams were used to obtain lists of overlapping and nonoverlapping DCMs between distinct two-group comparisons. Bar plots were generated and two-way ANOVA statistical tests were performed for each metabolite to compare metabolite abundances across genotypes and treatment conditions. Pairwise Student's *t*-tests, two-way ANOVA statistical analysis, metabolite enrichment visualizations, and heat maps for DCMs of interest were performed in GRAPHPAD PRISM (Boston, MA, USA), version 10.2.

Acknowledgements

This work was supported by the National Institutes of Health (NIH) Minnesota Muscle Training Grant [5T32AR007612-21, 5T32AR007612-22] to EJ, the NIH Functional Proteomics of Aging Training Grant [5T32AG029796-13, 5T32AG029796-14] to EJ, and by NIH grants [5R01AR042423-27] and [5R01AR049899-18] to JME.

Conflict of interest

The authors declare no conflict of interest.

Author contributions

EEJ and JME conceived the study and designed experiments; EEJ performed experiments, analyzed data, and wrote the manuscript; EEJ and JME made manuscript revisions.

Peer review

The peer review history for this article is available at https://www.webofscience.com/api/gateway/wos/peer-review/10.1111/febs.70029.

Data availability statement

These data are available at the NIH Common Fund's National Metabolomics Data Repository (NMDR) website, the Metabolomics Workbench, https://www.metabolomicsworkbench.org where it has been assigned Project ID ST003335. The data can be accessed directly via its Project DOI: https://doi.org/10.21228/M8HZ53. R script used to generate plots and filter data is publicly available at: https://github.com/joh18358/Stress-metabolomics-analysis. This work is supported by Metabolomics Workbench/National Metabolomics Data Repository (NMDR) (grant# U2C-DK119886), Common Fund Data Ecosystem (CFDE) (grant# 3OT2OD030544), and Metabolomics Consortium Coordinating Center (M3C) (grant# 1U2C-DK119889).

References

1 Sekiguchi M, Zushida K, Yoshida M, Maekawa M, Kamichi S, Yoshida M, Sahara Y, Yuasa S, Takeda S & Wada K (2009) A deficit of brain dystrophin impairs specific amygdala GABAergic transmission and enhances defensive behaviour in mice. *Brain* **132**, 124–135.

2 Vaillend C & Chaussenot R (2017) Relationships linking emotional, motor, cognitive and GABAergic dysfunctions in dystrophin-deficient mdx mice. *Hum Mol Genet* **26**, 1041–1055.

3 Lindsay A & Russell AP (2023) The unconditioned fear response in dystrophin-deficient mice is associated with adrenal and vascular function. *Sci Rep* **13**, 5513.

4 Zarrouki F, Goutal S, Vacca O, Garcia L, Tournier N, Goyenvalle A & Vaillend C (2022) Abnormal expression of synaptic and extrasynaptic GABAA receptor subunits in the dystrophin-deficient mdx mouse. *Int J Mol Sci* **23**, 12617.

5 Goyenvalle A, Griffith G, Babbs A, El Andaloussi S, Ezzat K, Avril A, Dugovic B, Chaussenot R, Ferry A, Voit T *et al.* (2015) Functional correction in mouse models of muscular dystrophy using exon-skipping tricyclo-DNA oligomers. *Nat Med* **21**, 270–275.

6 Razzoli M, Lindsay A, Law M, Chamberlain CM, Southern WM, Berg M, Osborn J, Engeland W, Metzger JM, Ervasti JM *et al.* (2020) Social stress is lethal in the mdx model of Duchenne muscular dystrophy. *EBioMedicine* **55**, 102700.

7 Johnson EE, Southern WM, Doud B, Steiger B, Razzoli M, Bartolomucci A & Ervasti JM (2024) Retention of stress susceptibility in the mdx mouse model of Duchenne muscular dystrophy after PGC-1α overexpression or ablation of IDO1 or CD38. *Hum Mol Genet* **26**, 312–318.

8 Maresh K, Papageorgiou A, Ridout D, Harrison NA, Mandy W, Skuse D & Muntoni F (2023) Startle responses in Duchenne muscular dystrophy: a novel biomarker of brain dystrophin deficiency. *Brain* **146**, 252–265.

9 Gharibi S, Vaillend C & Lindsay A (2024) The unconditioned fear response in vertebrates deficient in dystrophin. *Prog Neurobiol* **235**, 102590.
10 Saoudi A, Barberat S, le Coz O, Vacca O, Doisy Caquant M, Tensorer T, Sliwinski E, Garcia L, Muntoni F, Vaillend C *et al*. (2023) Partial restoration of brain dystrophin by tricyclo-DNA antisense oligonucleotides alleviates emotional deficits in mdx52 mice. *Mol Ther Nucleic Acids* **32**, 173–188.
11 Lindsay A, Holm J, Razzoli M, Bartolomucci A, Ervasti JM & Lowe DA (2021) Some dystrophy phenotypes of dystrophin-deficient mdx mice are exacerbated by mild, repetitive daily stress. *FASEB J* **35**, e21489.
12 Matthews E, Brassington R, Kuntzer T, Jichi F & Manzur AY (2016) Corticosteroids for the treatment of Duchenne muscular dystrophy. *Cochrane Database Syst Rev* **2016**, CD003725.
13 Guglieri M, Bushby K, McDermott MP, Hart KA, Tawil R, Martens WB, Herr BE, McColl E, Speed C, Wilkinson J *et al*. (2022) Effect of different corticosteroid dosing regimens on clinical outcomes in boys with Duchenne muscular dystrophy: a randomized clinical trial. *JAMA* **327**, 1456–1468.
14 Panza E, Vellecco V, Iannotti FA, Paris D, Manzo OL, Smimmo M, Mitilini N, Boscaino A, de Dominicis G, Bucci M *et al*. (2021) Duchenne's muscular dystrophy involves a defective transsulfuration pathway activity. *Redox Biol* **45**, 102040.
15 Terrill JR, Grounds MD & Arthur PG (2015) Taurine deficiency, synthesis and transport in the mdx mouse model for Duchenne muscular dystrophy. *Int J Biochem Cell Biol* **66**, 141–148.
16 Lorena MDSV, Santos EKD, Ferretti R, Nagana Gowda GA, Odom GL, Chamberlain JS & Matsumura CY (2023) Biomarkers for Duchenne muscular dystrophy progression: impact of age in the mdx tongue spared muscle. *Skelet Muscle* **13**, 1–13.
17 Merckx C & De Paepe B (2022) The role of taurine in skeletal muscle functioning and its potential as a supportive treatment for Duchenne muscular dystrophy. *Metabolites* **12**, 193.
18 Sun Q, Wang B, Li Y, Sun F, Li P, Xia W, Zhou X, Li Q, Wang X, Chen J *et al*. (2016) Taurine supplementation lowers blood pressure and improves vascular function in prehypertension: randomized, double-blind, placebo-controlled study. *Hypertension* **67**, 541–549.
19 Lushchak VI (2012) Glutathione homeostasis and functions: potential targets for medical interventions. *J Amino Acids* **2012**, 736837.
20 Petrillo S, Pelosi L, Piemonte F, Travaglini L, Forcina L, Catteruccia M, Petrini S, Verardo M, D'Amico A, Musaró A *et al*. (2017) Oxidative stress in Duchenne muscular dystrophy: focus on the NRF2 redox pathway. *Hum Mol Genet* **26**, 2781–2790.
21 Surai PF, Earle-payne K & Kidd MT (2021) Taurine as a natural antioxidant: from direct antioxidant effects to protective action in various toxicological models. *Antioxidants Basel* **10**, 1876.
22 Sullivan RT, Lam NT, Haberman M, Beatka MJ, Afzal MZ, Lawlor MW & Strande JL (2021) Cardioprotective effect of nicorandil on isoproterenol induced cardiomyopathy in the mdx mouse model. *BMC Cardiovasc Disord* **21**, 1–12.
23 Lindsay A, McCourt PM, Karachunski P, Lowe DA & Ervasti JM (2018) Xanthine oxidase is hyper-active in Duchenne muscular dystrophy. *Free Radic Biol Med* **129**, 364–371.
24 Berdeaux R & Stewart R (2012) Intracellular signal for skeletal muscle adaptation: cAMP signaling in skeletal muscle adaptation: hypertrophy, metabolism, and regeneration. *Am J Physiol Endocrinol Metab* **303**, E1–E17.
25 Yan K, Gao LN, Cui YL, Zhang Y & Zhou X (2016) The cyclic AMP signaling pathway: exploring targets for successful drug discovery (review). *Mol Med Rep* **13**, 3715–3723.
26 Rezende B, Alencar AKN, de Bem GF, Fontes-Dantas FL & Montes GC (2023) Endocannabinoid system: chemical characteristics and biological activity. *Pharmaceuticals (Basel)* **16**, 148.
27 Grevengoed TJ, Trammell SAJ, McKinney MK, Petersen N, Cardone RL, Svenningsen JS, Ogasawara D, Nexøe-Larsen CC, Knop FK, Schwartz TW *et al*. (2019) N-acyl taurines are endogenous lipid messengers that improve glucose homeostasis. *Proc Natl Acad Sci USA* **116**, 24770–24778.
28 Argenziano M, Pota V, Di Paola A, Tortora C, Marrapodi MM, Giliberti G, Roberti D, Pace MC & Rossi F (2023) CB2 receptor as emerging anti-inflammatory target in Duchenne muscular dystrophy. *Int J Mol Sci* **24**, 3345.
29 Mann G, Mora S, Madu G & Adegoke OAJ (2021) Branched-chain amino acids: catabolism in skeletal muscle and implications for muscle and whole-body metabolism. *Front Physiol* **12**, 702826.
30 Quattrocelli M, Zelikovich AS, Jiang Z, Peek CB, Demonbreun AR, Kuntz NL, Barish GD, Haldar SM, Bass J & McNally EM (2019) Pulsed glucocorticoids enhance dystrophic muscle performance through epigenetic-metabolic reprogramming. *JCI Insight* **4**, e132402.
31 Zelikovich AS, Quattrocelli M, McNally EM & Kuntz NL (2020) Improved metabolic and bone health in boys with Duchenne muscular dystrophy treated with high dose pulse weekend corticosteroids compared to daily dosing (21). *Neurology* **94**(15_suppl), 21.
32 Martins-Bach AB, Bloise AC, Vainzof M & Rahnamaye Rabbani S (2012) Metabolic profile of dystrophic mdx mouse muscles analyzed with in vitro magnetic resonance spectroscopy (MRS). *Magn Reson Imaging* **30**, 1167–1176.

33 Pedley AM & Benkovic SJ (2016) A new view into the regulation of purine metabolism – the purinosome. *Trends Biochem Sci* **42**, 141.
34 Simoni RE, Ferreira Gomes LNL, Scalco FB, Oliveira CPH, Aquino Neto FR & Costa de Oliveira ML (2007) Uric acid changes in urine and plasma: an effective tool in screening for purine inborn errors of metabolism and other pathological conditions. *J Inherit Metab Dis* **30**, 295–309.
35 de Bruyn CH, Kulakowski S, van Bennekom CA, Renoirte P & Müller MM (1980) Purine metabolism in Duchenne muscular dystrophy. *Adv Exp Med Biol* **122A**, 177–182.
36 Timpani CA, Hayes A & Rybalka E (2015) Revisiting the dystrophin-ATP connection: how half a century of research still implicates mitochondrial dysfunction in Duchenne muscular dystrophy aetiology. *Med Hypotheses* **85**, 1021–1033.
37 Soslow JH, Markham LW, Burnette BW, Galindo CL, Feoktistov I, Raucci FJ, Damon BM, Sawyer DB & Ryzhov S (2017) Increased number of circulating CD8/CD26 T cells in the blood of duchenne muscular dystrophy patients is associated with augmented binding of adenosine deaminase and higher muscular strength scores. *Front Pharmacol* **8**, 914.
38 Saghatelian A, McKinney MK, Bandell M, Patapoutian A & Cravatt BF (2006) A FAAH-regulated class of N-acyl taurines that activates TRP ion channels. *Biochemistry* **45**, 9007–9015.
39 Kalkan H, Pagano E, Paris D, Panza E, Cuozzo M, Moriello C, Piscitelli F, Abolghasemi A, Gazzerro E, Silvestri C *et al*. (2023) Targeting gut dysbiosis against inflammation and impaired autophagy in Duchenne muscular dystrophy. *EMBO Mol Med* **15**, e16225.
40 Hillard CJ, Beatka M & Sarvaideo J (2016) Endocannabinoid signaling and the hypothalamic-pituitary-adrenal axis. *Compr Physiol* **7**, 1–15.
41 Iannotti FA, Pagano E, Guardiola O, Adinolfi S, Saccone V, Consalvi S, Piscitelli F, Gazzerro E, Busetto G, Carrella D *et al*. (2018) Genetic and pharmacological regulation of the endocannabinoid CB1 receptor in Duchenne muscular dystrophy. *Nat Commun* **9**, 3950.
42 Hu B, Doods H, Treede RD & Ceci A (2009) Depression-like behaviour in rats with mononeuropathy is reduced by the CB2-selective agonist GW405833. *Pain* **143**, 206–212.
43 Beins EC, Beiert T, Jenniches I, Hansen JN, Leidmaa E, Schrickel JW & Zimmer A (2021) Cannabinoid receptor 1 signalling modulates stress susceptibility and microglial responses to chronic social defeat stress. *Transl Psychiatry* **11**, 164.
44 Al-Khalili Szigyarto C & Spitali P (2018) Biomarkers of Duchenne muscular dystrophy: current findings. *Degener Neurol Neuromuscul Dis* **8**, 1–13.
45 Lindsay A, Trewin AJ, Sadler KJ, Laird C, Della Gatta PA & Russell AP (2021) Sensitivity to behavioral stress impacts disease pathogenesis in dystrophin-deficient mice. *FASEB J* **35**, e22034.
46 Lindsay A, Chamberlain CM, Witthuhn BA, Lowe DA & Ervasti JM (2019) Dystrophinopathy-associated dysfunction of Krebs cycle metabolism. *Hum Mol Genet* **28**, 942–951.
47 Srivastava NK, Annarao S & Sinha N (2016) Metabolic status of patients with muscular dystrophy in early phase of the disease: in vitro, high resolution NMR spectroscopy based metabolomics analysis of serum. *Life Sci* **151**, 122–129.
48 Xu H, Cai X, Xu K, Wu Q & Xu B (2023) The metabolomic plasma profile of patients with Duchenne muscular dystrophy: providing new evidence for its pathogenesis. *Orphanet J Rare Dis* **18**, 273.
49 Taschetto L, Scaini G, Zapelini HG, Ramos ÂC, Strapazzon G, Andrade VM, Réus GZ, Michels M, Dal-Pizzol F, Quevedo J *et al*. (2017) Acute and long-term effects of intracerebroventricular administration of α-ketoisocaproic acid on oxidative stress parameters and cognitive and noncognitive behaviors. *Metab Brain Dis* **32**, 1507–1518.
50 Wisniewski MSW, Carvalho-Silva M, Gomes LM, Zapelini HG, Schuck PF, Ferreira GC, Scaini G & Streck EL (2016) Intracerebroventricular administration of α-ketoisocaproic acid decreases brain-derived neurotrophic factor and nerve growth factor levels in brain of young rats. *Metab Brain Dis* **31**, 377–383.
51 Murashige D, Jung JW, Neinast MD, Levin MG, Chu Q, Lambert JP, Garbincius JF, Kim B, Hoshino A, Marti-Pamies I *et al*. (2022) Extra-cardiac BCAA catabolism lowers blood pressure and protects from heart failure. *Cell Metab* **34**, 1749–1764.e7.
52 Belanto JJ, Olthoff JT, Mader TL, Chamberlain CM, Nelson M, Mccourt PM, Talsness DM, Gundersen GG, Lowe DA & Ervasti JM (2016) Independent variability of microtubule perturbations associated with dystrophinopathy. *Hum Mol Genet* **25**, 4951–4961.
53 Ford L, Kennedy AD, Goodman KD, Pappan KL, Evans AM, Miller LAD, Wulff JE, Wiggs BR, Lennon JJ, Elsea S *et al*. (2020) Precision of a clinical metabolomics profiling platform for use in the identification of inborn errors of metabolism. *J Appl Lab Med* **5**, 342–356.

Supporting information

Additional supporting information may be found online in the Supporting Information section at the end of the article.

Data S1. Metabolon Biological Stress Targeted Metabolomics Data.